

Levels of nonuniformity less than 1% have been found at the critical surface. The nonuniformity may be reduced even further by lateral thermal transport as heat flows from the critical surface to the ablation surface. Even with the small separation between these surfaces expected for short-wavelength laser irradiation (0.35  $\mu\text{m}$ ), adequate thermal smoothing is possible due to the relatively small spatial wavelengths of the nonuniformities.

Finally, it has been shown that high uniformity can be obtained using the high-f-number optics (subtending less than 2% of the total solid angle) that will be required for future fusion reactors.

#### REFERENCES

1. J. H. Nuckolls, L. Wood, A. Thiessen, and G. Zimmerman, *Nature* **239**, 139 (1972).
2. W. C. Mead and J. D. Lindl, LLNL Report UCRL-78459 (1976).
3. M. H. Emery, J. H. Orens, J. H. Gardner, and J. P. Boris, *Phys. Rev. Lett.* **48**, 253 (1982).
4. R. G. Evans, A. J. Bennett, and G. J. Pert, *J. Phys. D* **15**, 1673 (1982).
5. S. Skupsky and K. Lee, LLE Report 137, submitted for publication to *Journal of Applied Physics*.
6. M. J. Monsler, J. Hovingh, D. L. Cook, T. G. Frank, and G. A. Moses, *Nucl. Technol./Fusion* **1**, 302 (1981).
7. C. E. Max, C. F. McKee, and W. C. Mead, *Phys. Fluids* **23**, 1620 (1980).
8. LLE Review **12**, 5 (1982).
9. S. E. Bodner, *J. Fusion Energy* **1**, 221 (1981).

## 2.B Thermal Transport Measurements on OMEGA

Transport experiments have been conducted on the 24-beam OMEGA laser system under conditions of uniform spherical irradiation. Thermal transport in spherical geometry has been found to differ from transport under comparable single-beam target-irradiation conditions, and cannot be described in terms of a flux-inhibited model. We have found on OMEGA that electrons in the tail of the thermal velocity distribution deposit energy deep into the target, leading to a temperature profile which is less steep than predicted by a flux-inhibited model.

Thermal transport is one of the crucial processes affecting target performance in laser fusion. Many experiments to determine transport have been conducted in single-beam irradiation geometry; on GDL, for example, inhibited transport consistent with a flux limiter of 0.03-0.05 was found for 0.35- $\mu\text{m}$  irradiation.<sup>1</sup> Recent spherical irradiation experiments at the Rutherford Laboratory<sup>2</sup> have, however, indicated less inhibited transport than most single-beam experiments, and suggested a higher value of 0.1 for the flux limiter.

Thermal transport can be deduced from "burn-through" measurements on simple layered targets comprising a layer of ablator material (e.g., plastic) coated onto a substrate. The intensity of appropriate x-ray lines from the substrate layer is measured for various overcoat-layer thicknesses and comparison is made with code predictions. A high degree of uniformity is essential when comparing experimental transport results with a one-dimensional code. This is available on OMEGA: by focusing at a point which is about eight target radii behind the target center (tangential focus), the resulting rms intensity nonuniformity of the 24 overlapping beams is smaller than 6%.

The targets used in this study were thin glass shells of diameter  $\sim 400 \mu\text{m}$ , coated with a  $2\text{-}\mu\text{m}$ -thick copper layer, a "substrate" layer (Al, Ni, or Ti), and varying thicknesses of ablator material (parlyene). The copper coating made the target sufficiently massive to ensure that the transport issue would not be complicated by hydrodynamic motion. The substrate layer provided signature x-ray emission, measured with x-ray Bragg spectrographs and spectrally resolving x-ray streak cameras.

Figure 8 shows burn-through curves for various incident (and absorbed) irradiances. The intensity of the  $2p\text{-}1s$  line of  $\text{Al}^{+12}$  at  $1.73 \text{ keV}$

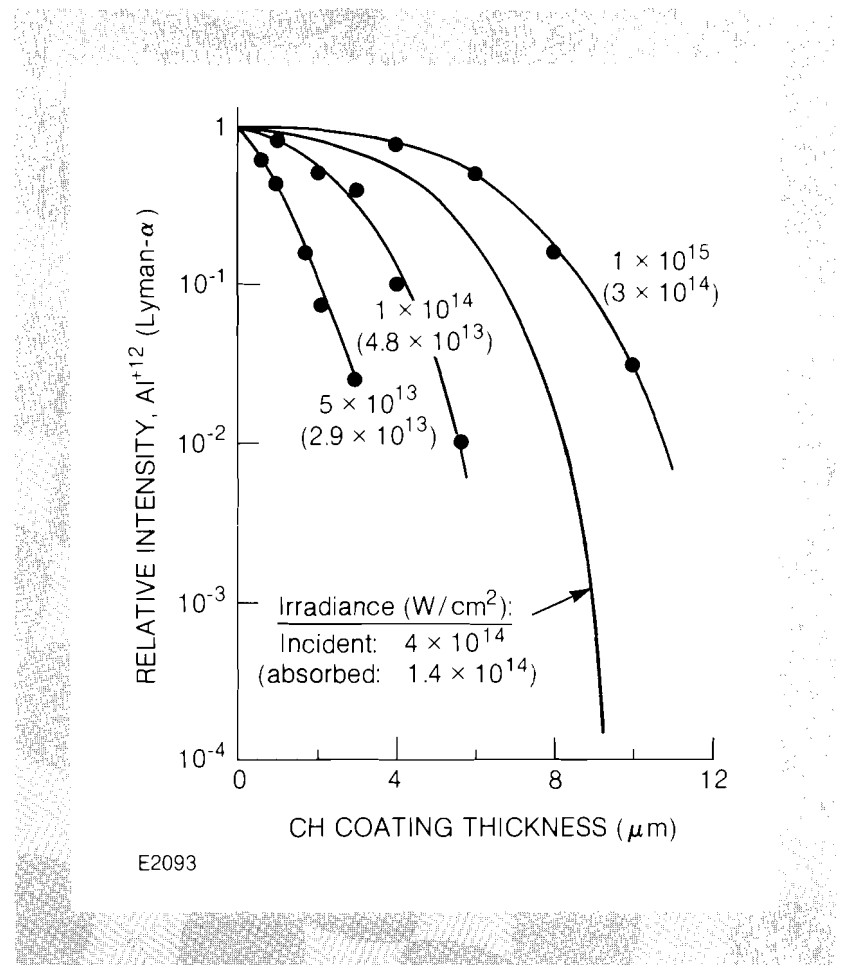
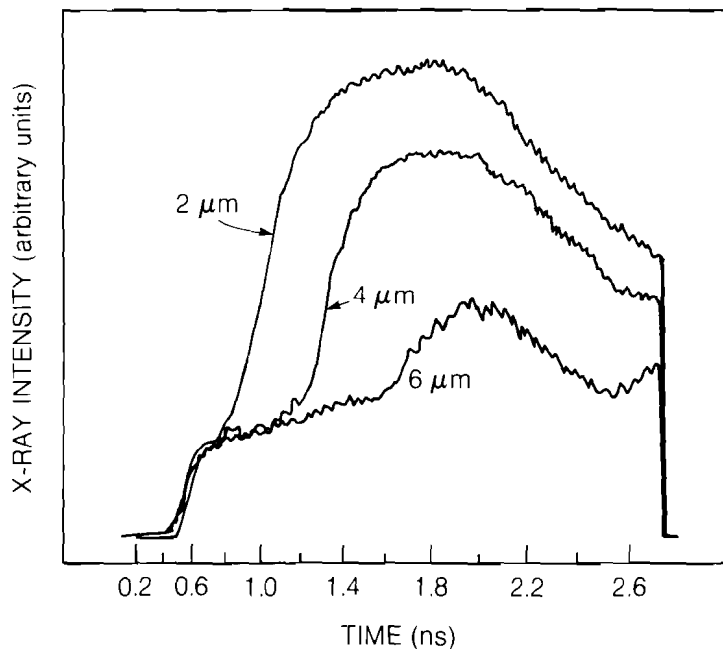
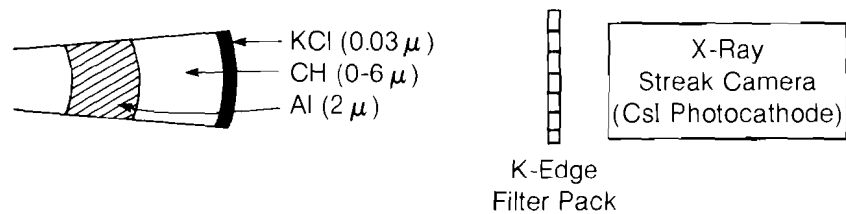


Fig. 8  
Transport is studied by measuring the x-ray signal from an aluminum substrate coated with various thicknesses of parlyene (CH). Greater thicknesses of parlyene are burnt through at higher intensities. The mass-ablation rate may be estimated by dividing the burn depth by the laser pulse width.

Fig. 9

X-ray streak traces for different CH coating thicknesses, at  $4 \times 10^{14}$  W/cm<sup>2</sup>. The filter in front of the camera selects the photon energy range  $\sim 2$ -2.8 keV which includes the aluminum line used in Fig. 8. The first rise in intensity (at 0.5 ns) marks the heating of the KCl surface layer. The second rise is due to penetration into the aluminum substrate. The mass-ablation rate may be estimated directly from the times of onset of this second rise in successive traces.

is plotted against the thickness of the parylene coating. For each case, the "penetration depth" is about three times larger than predicted by the one-dimensional laser fusion code *LILAC* for a flux limiter  $f = 0.03$ -0.05; it is comparable to what is predicted for no flux limitation ( $f = 0.65$ ), but in this case the calculated absorption fraction is too high by a factor of two. The fact that no intensity threshold is observed for this departure from theory suggests that this discrepancy is not caused by an instability, such as filamentation which would lead to nonuniform heat penetration. This conclusion is supported by x-ray streak-camera measurements (Fig. 9) which show that the sharp rise in intensity (due to penetration into the substrate) occurs progressively later in time for thicker parylene thicknesses. With filamentation, we would expect this rise to occur near the peak of the pulse; in contrast, for the 6- $\mu$ m case this rise occurs when the laser pulse is practically over.



E2233

Since the present results for uniform, spherical irradiation are markedly different from most reported results for single-beam, plane-target irradiation, we have compared the uniform and nonuniform irradiation of spherical targets at the same incident irradiance (see Fig. 10). We used two additional geometries: (a) one single beam (of the 24 OMEGA beams) was focused to a 150- $\mu\text{m}$ -diameter spot on spherical targets, and (b) all 24 beams were focused to small discrete spots, of diameter 70  $\mu\text{m}$ , on the surfaces of spherical targets. The incident irradiance in all these cases was adjusted to the same approximate value of  $4 \times 10^{14} \text{ W/cm}^2$ . The nonuniform irradiance curve in Fig. 10 fits both cases (a) and (b), and agrees with a LILAC prediction assuming  $f=0.03$  and spherical symmetry. We are led to conclude that this agreement is fortuitous: there must be some two-dimensional effects which manifest themselves as an effective flux inhibition.

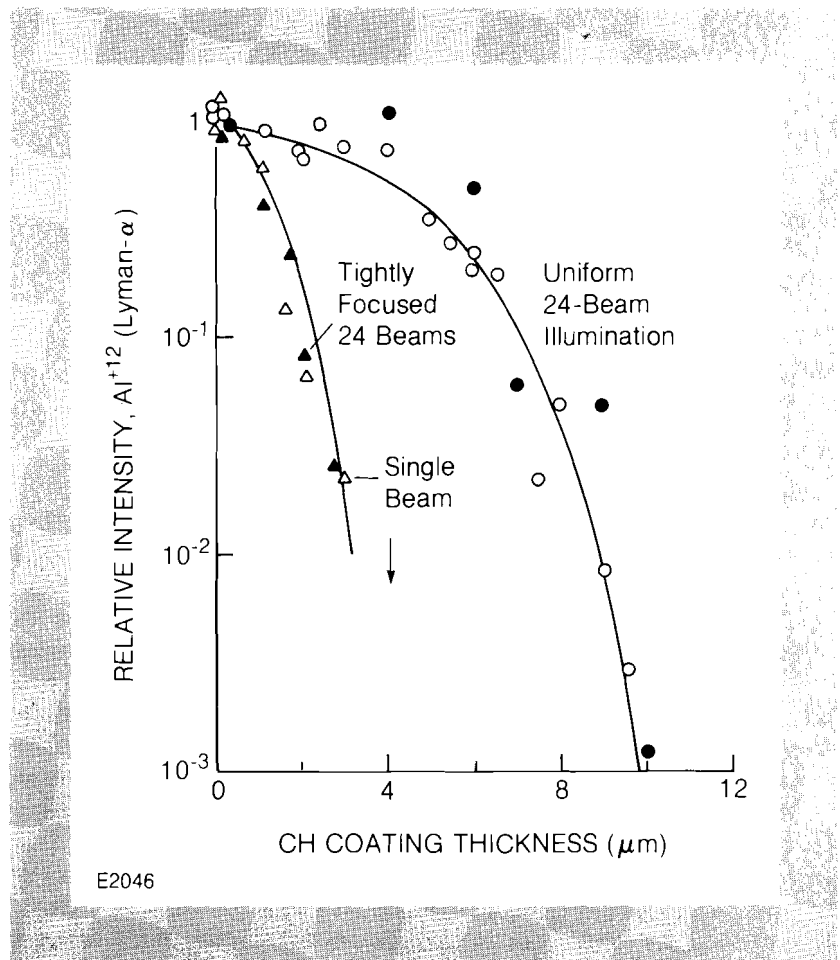
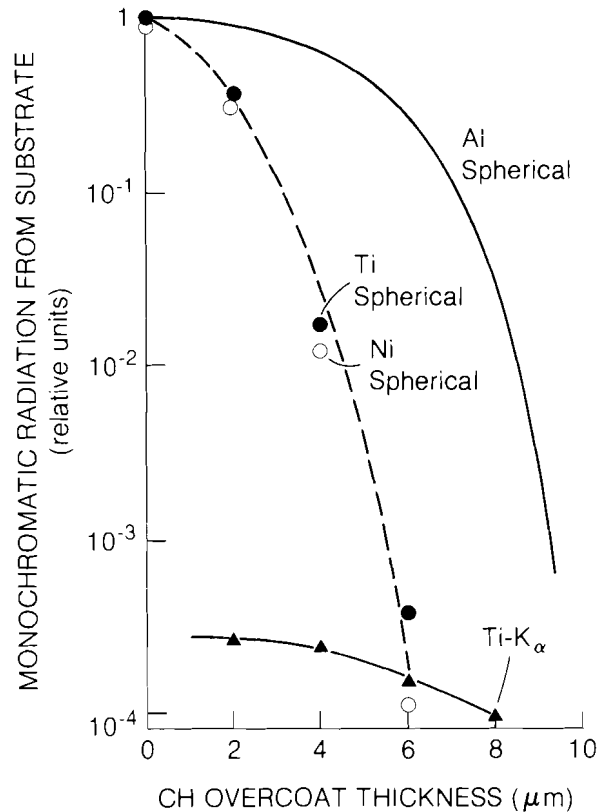


Fig. 10  
Comparison of burn-through for uniform and nonuniform irradiation of spherical targets. In each case the target was CH coated on aluminum, and the irradiance was approximately  $4 \times 10^{14} \text{ W/cm}^2$ . The arrow indicates a coating thickness for which the x-ray signal was below the threshold for detectability. The different curves were separately normalized to 1. The full and empty circles pertain to two separate series of experiments, demonstrating the reproducibility of the results.

Mapping of the heat-front temperature profile is essential to the understanding of transport in spherical geometry. We have extended these burn-through measurements using higher-atomic-number substrates, titanium and nickel. Figure 11 summarizes the results for an incident irradiance of  $4 \times 10^{14} \text{ W/cm}^2$ . The aluminum line at 1.73 keV probes temperature contours near 400 eV, while the corresponding titanium line at 4.75 keV and the nickel line at 7.8 keV probe higher temperatures, near 1 keV and 1.5 keV respectively. The marked dif-

Fig. 11

Burn-through of parylene coating for substrates of different  $Z$  (aluminum, titanium, and nickel), at  $4 \times 10^{14} \text{ W/cm}^2$ . The higher- $Z$  elements indicate a smaller burn depth, since the x-ray lines used are excited at higher temperatures. The titanium  $K_\alpha$  yield, indicative of the preheat of cold material by fast electrons, is also shown.



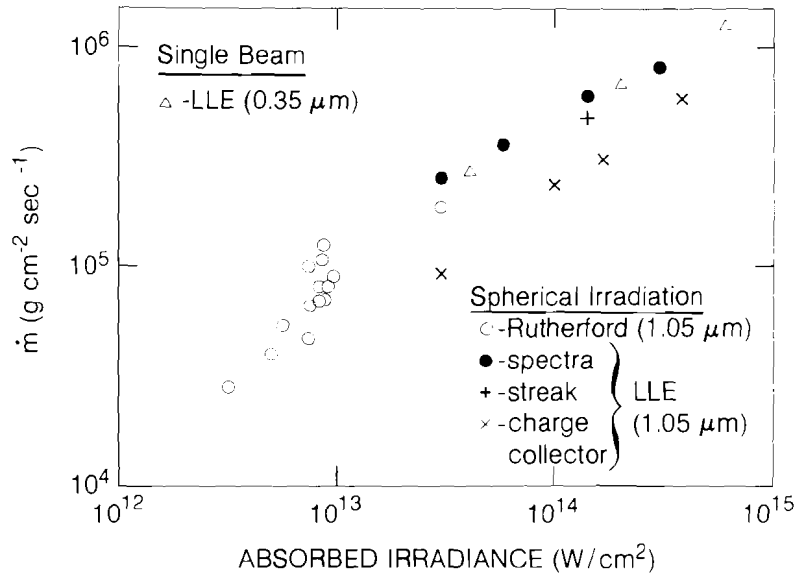
E2107

ference between the low- $Z$  and high- $Z$  burn-through curves is evidence of a very gradual temperature fall at the heat front. It shows the inapplicability of the flux-limited model (with any  $f$ ), or even the classical uninhibited model; both these models predict a very steep heat front, and a burn-through curve almost independent of substrate material. There is probably penetration of only a "foot" of relatively low temperature ahead of the heat front into the higher-density, deeper target layers. The rest of the heat front may still be described by flux-inhibited transport.

Figure 11 also shows the intensity of  $K_\alpha$  lines from the high- $Z$  substrate which are indicative of preheat by fast electrons. Using the absolute magnitude of the  $K_\alpha$  line intensities, we would estimate<sup>3</sup> that only about 0.7% of the absorbed energy at  $10^{15} \text{ W/cm}^2$  is deposited as fast-electron preheat. This, however, may be misleading: resonance-absorption electrons which move inwards from the critical layer encounter a layer of thickness of the order of their range which is already heated by the penetrating "foot" of the heat front. The emission of  $K_\alpha$  radiation, which requires cold material, is therefore thwarted. In other words, the preheat is actually higher than deduced from the  $K_\alpha$  line.

Burn-through curves (see Fig. 8) can be used to obtain the peak

mass-ablation rate. The total mass ablated is taken as that corresponding to the maximum penetration of the aluminum emission curves in Fig. 8. After dividing by the pulse width and applying a small correction factor<sup>4</sup> we arrive at the results shown in Fig. 12 (solid points).



E2234

Fig. 12 Comparison of mass-ablation rates as a function of absorbed irradiance. Results marked by solid circles were obtained from the burn-through curves in Fig. 8; + —by streak traces (see Fig. 9); x—by charge-collector signals. Results obtained at LLE and the Rutherford Laboratory are consistent.

The streak-camera results (Fig. 9) allow the mass-ablation rate to be estimated directly by taking the time difference of the onset of the second rise in successive traces. For example, for the 2- $\mu\text{m}$  and 4- $\mu\text{m}$  coating thicknesses, this onset occurs near 0.8 and 1.2 ns, respectively.

The mass-ablation rate can alternatively be determined from the average ion velocity as measured by charge collectors. If  $E_a$  is the absorbed energy per unit area,  $V$  the ion expansion velocity, and  $\Delta t$  the pulse width, the mass-ablation rate is given approximately by  $\dot{m} = 2E_a/V^2\Delta t$ , where  $V^2$  is averaged over the distribution. The mass-ablation rate so derived is shown in Fig. 12 to be consistently lower than that derived spectroscopically. This indicates that the deep penetration of lower temperature contours does not contribute to mass ablation and hence to drive efficiency as much as if the entire heat front had penetrated to the same depth.

For comparison, we also show in Fig. 12 results obtained at the Rutherford Laboratory using spherical irradiation at  $\lambda = 1.05 \mu\text{m}$ ,<sup>2</sup> and results reported earlier by us using single-beam irradiation at  $\lambda = 0.35 \mu\text{m}$ .<sup>1</sup> Since  $\dot{m}$  for spherical irradiation was found to be about the same at different laser wavelengths (for the same absorbed irradiance),<sup>2</sup> we can expect from Fig. 12 that for  $\lambda = 0.35 \mu\text{m}$ ,  $\dot{m}$  would be